Atmos. Chem. Phys. Discuss., 10, 9369–9389, 2010
www.atmos-chem-phys-discuss.net/10/9369/2010/

Atmospheric Chemistry and Physics Discussions

This discussion paper is/has been under review for the journal Atmospheric Chemistry and Physics (ACP). Please refer to the corresponding final paper in ACP if available.

Optical-chemical relationships for carbonaceous aerosols observed at Jeju Island, Korea with a 3-laser photoacoustic spectrometer

B. A. Flowers[1], M. K. Dubey[1], C. Mazzoleni[2], E. A. Stone[3], J. J.. Schauer[3], and S.-W. Kim[4]

[1]Earth and Environmental Science Division, Los Alamos National Laboratory, Los Alamos, NM 87545, USA
[2]Department of Physics, Michigan Technological University, Houghton, MI 49931, USA
[3]Environmental Chemistry and Technology, University of Wisconsin-Madison, Madison, WI 53706, USA
[4]Seoul National University, Seoul, South Korea

Received: 29 March 2010 – Accepted: 6 April 2010 – Published: 14 April 2010

Correspondence to: B. A. Flowers (bflowers@lanl.gov)

Published by Copernicus Publications on behalf of the European Geosciences Union.

Abstract

Transport of aerosols in pollution plumes from the mainland Asian continent was observed in situ at Jeju, South Korea during the Cheju Asian Brown Cloud Plume-Asian Monsoon Experiment (CAPMEX) field campaign throughout August and September 2008 using a 3-laser photoacoustic spectrometer. Transport of mixed sulfate, carbonaceous, and nitrate aerosols from various Asian pollution plumes to Jeju accounted for 76% of the deployment days, showing large variations in their measured chemical and optical properties. Our analysis of eight distinct episodes, spanning a wide range of chemical composition, optical properties, and source regions, reveals that at episodes with higher OC/SO_4^{2-} and NO_3^-/SO_4^{2-} composition ratios exhibit lower single scatter albedo at shorter wavelengths (ω_{405}); significantly lower [$\omega_{405}^{meas} = 0.79 \pm 0.06$, $\omega_{405}^{calc} = 0.86 \pm 0.01$] than predicted by an optical model that assumes constant complex index of refraction with wavelength (an optical model of soot). We attribute this discrepancy to enhanced absorption by organic material. Organic carbon absorption accounts for up to 50% of the measured aerosol absorption at 405 nm for the high OC/SO_4^{2-} episode. Coatings of elemental carbon aerosol cores are hypothesized to increase absorption by factors up to 6 at visible wavelengths. Carbonaceous aerosol absorption can alter global radiative forcing estimates substantially, underscoring the need to understand and predict chemical composition effects on optical properties.

1 Introduction

Understanding long-range transport (LRT) of pollutants is crucial to inform and implement international and/or regional policies on air-quality (UN-ECE, 2009) and climate change (IPCC, 2007) Outstanding issues include the quantification of aerosol radiative forcing, which depends on composition, mixing state, size, and morphology, as well as the attribution of sources of trans-boundary pollution including greenhouse gases. Carbonaceous (black carbon + organic, primary and secondary) aerosols found through-

ACPD
10, 9369–9389, 2010

out the atmosphere including in large scale Atmospheric Brown Clouds (ABCs) absorb solar radiation, warm the atmosphere, enhance snow pack and ice sheet melting, and suppress rainfall over vast polluted regions (Ramanathan and Carmichael, 2008) Large scale ABCs are prominent contributors to the continental Asian pollution plume, which entrains regional anthropogenic and natural emissions, whose composition changes with age as it is transported over the Pacific (Dunlea et al., 2009) Process level understanding of the optical properties of Asian aerosol outflow during its transport across distances up to thousands of kilometers lasting several days is essential to evaluate its radiative forcing in the region.

The CAPMEX field campaign was designed to monitor continental outflow from Asia and to observe the effect of Asian emissions and ABCs on atmospheric radiation especially during enforced air quality periods surrounding the summer 2008 Beijing Olympics (Ramanathan, 2009) The Gosan Observatory is located on the western side of Jeju Island, a resort island approximately 1100 km southeast of Beijing; and the Gosan Observatory is not affected by major local industrial pollution sources and has been used to observe continental outflow from Asia for several years (Chen et al., 1997; Clarke et al., 2004; Topping et al., 2004) In this paper we show correlations between simultaneous and independent measurements of aerosol optical properties and chemical composition at the Gosan site, in plumes undergoing transport from Asia and demonstrate some effects of chemical composition on aerosol light absorption.

2 Methods

A 3-laser photoacoustic spectrometer (PASS-3, Droplet Measurement Technologies, Inc., Boulder, CO), a commercial extension of prototypes originally developed at Desert Research Institute and the University of Nevada, Reno(Lewis et al., 2008), was used to measure aerosol absorption and scattering coefficients (β_{abs} and β_{sca}) at the Gosan Observatory. The PASS-3 uses 405, 532, and 781 nm diode lasers aligned in an acoustic resonator and measures aerosol absorption using the photoacoustic effect. The

detection limits (10 min signal integration) are 1.5 Mm^{-1} for β_{abs} and 2.0 Mm^{-1} for β_{sca} at 405 nm, 2.0 Mm^{-1} for β_{abs} and 3.0 Mm^{-1} for β_{sca} at 532 nm, and 0.15 Mm^{-1} for β_{abs} and 1.0 Mm^{-1} for β_{sca} at 781 nm (see supplementary information for a short description of PASS-3 calibration and performance characteristics and also (Cross et al., 2010) for laboratory comparison, http://www.atmos-chem-phys-discuss.net/10/9369/2010/acpd-10-9369-2010-supplement.pdf).

Elemental carbon (EC) and organic carbon (OC) mass were obtained daily from quartz-based filter measurements at the Gosan Observatory using thermal-optical and chemical methods (Schauer et al., 2003) The $PM_{2.5}$ mass was measured gravimetrically and sulfate was determined by ion-chromatography (Stone et al., 2007) Uncertainties for the organic carbon mass were ~0.20 μg m^{-3} and ~0.15 μg m^{-3} for elemental carbon.

The β_{sca} at 405 and 781 nm were used to calculate the intensive Ångström exponent of light scattering ($Å_{sca}^{405}$), which depends on particle size,

$$Å_{sca} = \frac{-\ln\left(\frac{\beta_{sca}(\lambda_1)}{\beta_{sca}(\lambda_2)}\right)}{\ln\left(\frac{\lambda_1}{\lambda_2}\right)} \quad (1)$$

where $\lambda_1 = 405$ nm and $\lambda_2 = 781$ nm. Smaller particles exhibit larger $Å_{sca}^{405}$. In order to diagnose the absorbing component of the aerosol, the Ångström exponent of β_{abs} (defined in complete analogy with (1) but for the absorption coefficient β_{abs}) at 405 relative to 532 nm, $Å_{abs}$(405/532), as well as $Å_{abs}$(405/781), were also calculated. The absorption wavelength dependence depends on carbonaceous particle composition because strong wavelength dependence ($Å_{abs}$>1.6) can indicate organic carbon absorption (Bond and Bergstrom, 2006; Gyawali et al., 2009; Lack and Cappa, 2010) Additionally the intensive single scatter albedo (ω_λ) were calculated using,

$$\omega_\lambda = \frac{\beta_{sca}(\lambda)}{[\beta_{abs}(\lambda) + \beta_{sca}(\lambda)]} \quad (2)$$

ACPD
10, 9369–9389, 2010

where λ refers to any one of the PASS-3 laser wavelengths.

NOAA HYSPLIT five-day back-trajectories for each day of the CPAMEX deployment are included in the supplementary information (http://www.atmos-chem-phys-discuss.net/10/9369/2010/acpd-10-9369-2010-supplement.pdf)to trace the path(s) the air mass had taken to Jeju and to assist in determination of the origin, evolution, and duration of each pollution transport episode (Draxler and Rolph, 2003) We discuss only the episodes in which we have both optical property and composition data.

3 Results and discussion

3.1 Optical properties

We expect aerosols undergoing transport from Asia to the Gosan Observatory to be well-mixed in aged air masses in which atmospheric processing over several days likely increases internal mixing of the aerosol components hereby producing more uniform intensive optical properties. The continuous observations of β_{sca} and β_{abs} at 405, 532, and 781 nm, the calculated (Å_{sca}^{405}) and ω_{405} for the CAPMEX deployment are shown in Fig. 1 and are used, along with back trajectories, to separate Asian transport from local pollution episodes.

In Fig. 1, aerosols arriving at Jeju during the periods highlighted in ash show enhanced extensive scattering and absorption signals and relatively uniform intensive properties Å_{sca}^{405} and ω_{405} compared to periods shown in white, which are dominated by local inputs, and/or precipitation events where β_{abs} and β_{sca} are low and the intensive optical properties are highly variable. We identify aerosol episodes occurring on 3, 6–8, 13–23, 27–31 August and 3–13, 16–20, 21–25, and 27–29 September (hence referred to as episodes 1–8) at Gosan stemming from transport of polluted Asian air masses (further evidenced by back trajectories). For the entire campaign, the mean β_{abs} at 405 nm during Asian transport episodes varies between 11 and 17 Mm^{-1} while β_{sca} varies between 42 and 411 Mm^{-1}. At 532 nm, the mean β_{abs} varies between 4 and

9 Mm^{-1} while mean β_{sca} varies between 23 and 280 Mm^{-1} and at 781 nm, mean β_{abs} varies between 3 and 5 Mm^{-1} while the mean β_{sca} varies between 17 and 188 Mm^{-1}.

We observe the Ångström exponent of absorption ($Å_{abs}$(405/781)) is nearly constant (mean values ~2.0) for all transport episodes, indicating significant presence of absorbing organic material in each episode. To further diagnose the absorbing organic component, we use the Ångström exponent of absorption ($Å_{abs}$(405/532)), where the wavelength dependence is strongly influenced by organic content and we expect to see strong increases in the wavelength dependence at short wavelengths corresponding to absorption by organic material. The Ångström exponents over both wavelength ranges are included with the optical properties in Table 1.

3.2 Chemical composition

Independent mass and chemical information was assembled from simultaneous analysis of aerosol collected on quartz filters from 24-hour periods during most of the campaign. The measured $PM_{2.5}$ total mass temporal profile (in μg m^{-3}) included in Fig. 1 agrees very well with the β_{sca} profile, independently separating Asian transport from local input periods. Also shown in Fig. 1 is the temporal profile of sulfate (SO_4^{2-}), ammonium (NH_4^+), OC, and EC as well the temporal profile of the OC/SO_4^{2-} ratio. We focus our discussion on OC/SO_4^{2-} and NO_3^- /SO_4^{2-} ratios as metrics for aerosol composition that vary significantly due to changes in source regions and the transport trajectory of the plumes (see Table 2).

The individual pollutants are enriched during transport episodes, though by varying amounts. The SO_4^{2-} mass (from the $PM_{2.5}$ fraction) changed the most, mean levels varied between 2.8 and 12.3 μg m^{-3}, while there was less variation in OC (1.1–1.9 μg m^{-3}) and NO_3^- (0.7–1.9 μg m^{-3}) in transport episodes. Episode 3 has the largest sulfate mass (12.3 μg m^{-3}) and the lowest OC/SO_4^{2-} and NO_3^-/SO_4^{2-} ratios. This is consistent with back trajectories originating, at early times, 13–16 August, from the South China Sea and at late times, 17–23 August, northeast of Jeju and becoming enriched

ACPD
10, 9369–9389, 2010

in sulfate pollution from southeastern China, an area influenced by a large number of power plants. The sulfate mass is comparable when compared with a similar episode reported by Topping et al. (2004) (14.48 $\mu g\,m^{-3}$ averaged over a 4 day episode originating in mainland China and passing through the southeastern part of China on its way to Jeju). Episode 8 exhibits the lowest sulfate mass (2.8 $\mu g\,m^{-3}$) and highest OC/SO_4^{2-} and NO_3^-/SO_4^{2-} ratios of any episode in the deployment. The back trajectories originate in Siberia, where approximately 75 forest fires burned between 24 and 30 September 2008 (FIRMS, 2009) We expect the fire-impacted air mass to be rich in organics, and to entrain nitrogen-rich urban pollution and a modest amount of sulfate as it traverses northeastern China, an area with a lower number of power plants. In both the ACE-Asia(Topping et al., 2004) and CAPMEX results presented here, the OC/SO_4^{2-} and NO_3^-/SO_4^{2-} ratios are also lowest for air masses originating east of Beijing and traveling through southeastern China along their path to Jeju and highest for air masses originating in Siberia and northeast China. Episodes 4-6 are intermediate in sulfate mass as well as OC/SO_4^{2-} and NO_3^-/SO_4^{2-} ratios, and followed circuitous trajectories through the Sea of Japan, traversing over Japan and Korea, as well as remote continental Asian locations (see Table 2). In the next section our analysis will show that enhancements in particle organic carbon and nitrate relative to sulfate lead to increased light absorption at short wavelengths, underscoring the importance of treating such chemical effects on optical properties explicitly in climate and chemistry models.

3.3 Optical property and composition correlations

We show the relationships between mean chemical composition (OC/SO_4^{2-} and NO_3^-/SO_4^{2-}) and the intensive optical properties ω_{405} and $Å_{abs}(405/532)$ for episodes 3-8 in Fig. 2. These empirical correlations provide clues to how chemical composition affects optical properties. The measured ω_{405} correlates inversely with the mean OC/SO_4^{2-} and NO_3^-/SO_4^{2-} ratios, for carbonaceous aerosol originating from a range of source regions. Episode 8 has the lowest ω_{405} and highest OC/SO_4^{2-} and NO_3^-/SO_4^{2-}

ACPD
10, 9369–9389, 2010

ratios; episode 3 exhibits the highest ω_{405} and lowest OC/SO_4^{2-} and NO_3^-/SO_4^{2-} ratios. Nitrate rich plumes originate from NO_x source regions where subsequent heterogeneous processing enriches particle phase nitrate. If organics are present in the plumes, there is potential to form organic nitrates in the particle phase. Organic nitrates are known to absorb light at short wavelengths and are likely processed to the particle phase during LRT of pollution plumes rich in organics and nitrogen species such as episode 8 (Jacobson, 1998)

The changes in mass of OC and NO_3^- are relatively small across the transport episodes, what changes significantly is the relative SO_4^{2-} percent composition (86% in episode 3, 44% in episode 8, see Table 2). The changes in composition influence the optical properties in pollution transport episodes observed during of CAPMEX. The decrease in ω_{405} could be attributed in part to reduction in particle size thereby decreasing β_{sca} and changing particle composition can also have significant effects. To separate these effects, both $Å_{sca}^{405}$ and $Å_{abs}(405/532)$ are plotted as functions of composition (OC/SO_4^{2-}) and included in Fig. 2. The increase in $Å_{abs}(405/532)$ observed with increasing OC fraction demonstrates that enhanced short wavelength absorption plays a major role in the reduction of ω_{405}. Furthermore, a similar strong positive trend exists (though not shown in Fig. 2) for $Å_{abs}(405/532)$ vs. NO_3^-/SO_4^{2-} ratios during transport episodes in CAPMEX. Large poly-aromatic hydrocarbons and nitrated PAH molecules exhibit electronic absorption bands in the visible and could potentially be significant in this case as products of heterogeneous atmospheric processing (Ruiz-Morales and Mullins, 2007) In contrast, we find that $Å_{sca}^{405}$ increases only slightly with increasing OC/SO_4^{2-}, indicating that these particles are somewhat smaller. This indicates that organic and nitrate-rich aged sulfate aerosols have a propensity to absorb more light in the blue causing reduction of ω_{405}.

ACPD
10, 9369–9389, 2010

3.4 Wavelength dependence of optical properties

Enhanced absorption by organic and nitrate rich aerosols is evident in the observed wavelength dependence of single scatter albedo, $\omega(\lambda)$ in Fig. 3. We have separated the data into three groups based on the measured OC/SO_4^{2-} ratio: high (episode 8), intermediate (episodes 4, 5, 6) and low (episodes 3, 7). The measured $\omega(\lambda)$ values are plotted using ± 1 σ standard deviations as error bars. This represents the real variability of ω for each episode, a quantity much larger than instrumental uncertainty underlying our ω measurements. The figure also shows Mie scattering theory calculations of the expected dependence of $\omega(\lambda)$ assuming a wavelength independent index of refraction (to neglect the absorption of organics at short wavelengths). The Mie calculations were performed using lognormal size distributions with variable (free parameters) mean particle diameters and geometric standard deviations and by changing the value of the real and imaginary parts of the index of refraction. To constrain the model outputs, we forced the calculation to approach the measured $\text{Å}_{\text{sca}}^{405}$ and the measured ω_{781} such that the square root of the summed square of the relative differences between model and measurements were below 2.5%. The choice of a 2.5% threshold was dictated by an error propagation analysis of the instrumental relative uncertainty (random errors only) at the mean optical signals measured during the different episodes and represents a conservative estimation at a 2σ level. These constraints resulted in the following ranges for the mean diamteter of the particles D_p, geometric standard deviation σ_p, real part of the index of refraction n_p, and imaginary part of the index of refraction k_p; a) low OC/SO_4^{2-}: $D_P = 0.37 \pm 0.18$, $\sigma_P = 1.34 \pm 0.26$, $n_P = 1.472 \pm 0.080$, $k_P = 0.0099 \pm 0.0050$; b) Medium OC/SO_4^{2-}: $D_P = 0.33 \pm 0.16$, $\sigma_P = 1.35 \pm 0.26$, $n_P = 1.481 \pm 0.080$, $k_P = 0.0311 \pm 0.0075$; c) High OC/SO_4^{2-}: $D_P = 0.35 \pm 0.16$, $\sigma_P = 1.31 \pm 0.26$, $n_P = 1.482 \pm 0.080$, $k_P = 0.014 \pm 0.0040$ where uncertainties represent half of the interval between maximum and minimum value of the sensitivity study. The full lines in Fig. 3 represent the average of the calculated values that fell below the 2.5% threshold, while the dashed lines represent

ACPD
10, 9369–9389, 2010

the maximum and minimum deviations. The lines indicate how $\omega(\lambda)$ may behave for an absorbing aerosol with an imaginary index of refraction that remains constant with wavelength. The deviations of the measurements from the modeled curves are in agreement with an increase in imaginary index of refraction with wavelength, especially at 405 nm; this could be due to the presence of absorbing organic compounds. We measure ω_{405} that is 10 % less than predicted (or 4x darker at 405 nm than black carbon) for Asian transport aerosol with high OC/SO_4^{2-} and NO_3^-/SO_4^{2-} ratios, providing direct in situ evidence for a relative absorption enhancement at 405 nm. The enhancement is insignificant for medium and low OC/SO_4^{2-} and NO_3^-/SO_4^{2-} ratios, which indicates that $\omega(\lambda)$ is controlled by the amount of OC, organic nitrates, NO_3^- and SO_4^{2-} in mixed carbonaceous aerosol, primarily at shorter wavelengths. Our in situ field $\omega(\lambda)$ observations provide a chemical basis for reports of enhanced short wave absorption in remote column radiance data made in Mexico City (Barnard et al., 2008) and laboratory vegetation combustion studies reported by (Lewis et al., 2008).

3.5 Brown carbon mass absorption cross section (MAC_{BrC}) and coating effects on elemental carbon MAC (MAC_{EC})

Finally, we use the chemical composition and wavelength dependent optical data to separate brown carbon, elemental carbon, and coating contributions to the total mass absorption cross section ($MAC_{total} = MAC_{EC} + MAC_{BrC}$) using an empirical model with idealized assumptions. We have calculated MAC_{total} by dividing the measured absorption by the sum of OC and EC mass for each episode [$MAC_{total} = \beta_{abs}^{meas}/(EC_{mass} + OC_{mass})$]. Coating effects on MAC_{EC} can be separated from pure MAC_{EC} using our measured EC_{mass} and reported MAC values (10.6±0.6 $m^2\,g^{-1}$ at 405 nm, 7.32±0.5 $m^2\,g^{-1}$ at 532 nm, 4.24±0.2 $m^2\,g^{-1}$ at 781 nm) for denuded soot collected in a recent laboratory study (Cross et al., 2010) For the CAPMEX data set, we multiply the MAC for denuded soot by our observed EC_{mass} to estimate the light absorption from pure elemental carbon ($\beta_{abs}^{est} = MAC_{denudedsoot} \times EC_{mass}^{meas}$) at each PASS-3 wavelength.

ACPD
10, 9369–9389, 2010

We then postulate that OC absorption is negligible at 781 and empirically determine a factor that best matches β_{abs}^{est} to our measured β_{abs}(781 nm); ($\beta_{abs}^{est} = f \times \beta_{abs}^{meas}$). We interpret f as the absorption enhancement factor for the coating and find this ranges from 3–6 (at 781 nm) for the transport episodes in CAPMEX and is attributed to enhanced absorption by clear and absorbing coatings on elemental carbon aerosol cores. Our values are much higher than the enhancement reported in limited observational studies (Cross et al., 2010; Schwarz et al., 2008) We hypothesize that large enhancements observed in CAPMEX can result from increasing coating thickness during aerosol transport and also the mixed carbonaceous aerosol can contain materials that absorb in the red (Garland et al., 2008; Gyawali et al., 2009). Using β_{abs}^{est} calculated at each PASS-3 wavelength, we also determine percent contributions of elemental carbon and elemental carbon coating to the overall β_{abs}^{meas} at each wavelength. We found that elemental carbon absorption and the coating effect accounted for 73% of β_{abs}(405 nm) in episode 7 and 99% of β_{abs}(532 nm) in episodes 5 and 8. The smallest coating effect was observed during episode 8 (33 % at 405 nm). The difference between our β_{abs}^{meas} (405 nm) and β_{abs}^{meas} (532 nm) compared to β_{abs}^{est} (at 405 and 532 nm) is attributed to brown carbon absorption (additional absorption than accounted for by the coating of elemental carbon cores) and determine MAC_{BrC} by dividing ($\beta_{abs}^{meas} - \beta_{abs}^{est}$) by OC_{mass}. We infer MAC_{BrC} that range between 2.1±0.1 and 3.4±0.1 $m^2\,g^{-1}$ at 405 nm and between 0±0.1 and 1.0±0.1 $m^2\,g^{-1}$ at 532 nm and that brown carbon accounts for up to 50% of β_{abs}(405 nm) in episode 8 and up to 20% of β_{abs}(532 nm) in episode 2. Table 3 exhibits the MAC_{BrC} and absorption fractions for each episode. Similar MACs for OC have been reported (Favez et al., 2009) and similar EC and OC contributions to total aerosol absorption have been observed (Barnard et al., 2008; Clarke et al., 2004) Our analysis describes how light absorption is enhanced by brown carbon directly and by coatings on elemental carbon cores, with the coating effect being pronounced at 405 and 532 nm for all episodes except for the fire-impacted episode 8. Our MAC results for brown and coated elemental carbon shoule be valuable for chemistry/transport models and to quantitatively determine their impacts on climate radiative forcing and

photochemistry.

4 Conclusion

Transport of absorbing carbonaceous aerosols accounted for 74% of the observation time on Jeju, South Korea in August and September 2008. We sampled a range of polluted air masses with varying amounts of particle carbon, sulfate, organics, and nitrate. Measured intensive optical properties are correlated with chemical composition observations. These empirical correlations provide clues to how aerosol chemical composition influences and moderates aerosol optical properties that will help develop prognostic treatments for models. Episodes with high OC/SO_4^{2-} and NO_3^-/SO_4^{2-} ratios exhibit lower than expected ω_{405}, when compared to a size resolved optical model assuming constant index of refraction with wavelength. Our findings underscore the manner in which OC can enhance light absorption by coating and mixing with EC and that OC absorption can account for a significant fraction of aerosol absorption at short visible wavelengths.

A recent study shows that a small reduction in global mean aerosol single scatter albedo (0.986 to 0.970 at 550 nm) from a higher absorbing carbonaceous fraction increases the net anthropogenic radiative forcing to $-0.3\,Wm^{-2}$ from $-0.5\,Wm^{-2}$ (Myhre, 2009) For a fire-impacted high OC/SO_4^{2-} episode in CAPMEX, we observed [$\omega_{405} = 0.79\pm0.05$, $\omega_{532} = 0.84\pm0.10$, $\omega_{781} = 0.83\pm0.11$] compared with mean [$\omega_{405} = 0.92\pm0.05$, $\omega_{532} = 0.94\pm0.06$, $\omega_{781} = 0.95\pm0.05$] observed during two low OC/SO_4^{2-} episodes. Chemical composition (both absorbing and non-absorbing, organic and inorganic components) significantly affects aerosol optical properties particularly at shorter wavelengths. Our results underscore the need to explicitly parameterize aerosol composition effects on optical properties in regional chemistry and climate models, particularly in the Asian outflow, whose composition is changing due to energy growth and clean air policies. Our chemical-optical relations and derived MACs for carbonaceous aerosols provide empirical parameterizations that enable such analysis by

ACPD
10, 9369–9389, 2010

modelers.

Acknowledgements. We gratefully acknowledge V. Ramanathan, M. V. Ramana (UCSD), and S. C. Yoon (SNU) for critical discussions, logistical assistance, and organization of the CAPMEX campaign. The authors thank John Walker (DMT) for instrument installation and field operation.

References

Barnard, J. C., Volkamer, R., and Kassianov, E. I.: Estimation of the mass absorption cross section of the organic carbon component of aerosol in the Mexico City metropolitan area, Atmos. Chem. Phys., 8, 6665–6679, 2008, http://www.atmos-chem-phys.net/8/6665/2008/.

Bond, T. C., and Bergstrom, R. W.: Light absorption by carbonaceous particles: An investigative review, Aerosol Sci. Technol., 40, 27–67, 2006.

CAPMEX: www.ramanathatan.ucsd.edu/capmex.html, 2009.

Chen, L.-L., Carmichael, G. R., Hong, M.-S., Ueda, H., Shim, S., Song, C. H., Kim, Y. P., Arimoto, R., Prospero, J., Savoie, D., Murano, K., Park, J. K., Lee, H.-G., and Kang, C.: Influence of continental outflow events on the aerosol composition at Cheju Island, South Korea, J. Geophys. Res., 102, 28551–28574, 1997.

Clarke, A. D., Shinozuka, Y., Kapustin, V. N., Howell, S., Huebert, B., Doherty, S., Anderson, T., Covert, D., Anderson, J., Hua, X., Moore, K. G., II, McNaughton, C., Carmichael, G., and Weber, R.: Size distributions and mixtures of dust and black carbon aerosol in asian outflow: Physiochemistry and optical properties, J. Geophys. Res., 109, D15S09, doi:10.1029/2003JD004378, 2004.

Cross, E. S., Onasch, T. B., Ahern, A., Wrobel, W., Slowik, J., Olfert, J., Lack, D., Massoli, P., Cappa, C., Schwarz, J., Spackman, R., Fahey, D., Sedlacek, A., Trimborn, A., Jayne, J., Freedman, A., Williams, L., Ng, N. L., Mazzoleni, C., Dubey, M., Brem, B., Kok, G., Subramanian, R., Freitag, S., Clarke, A., Thornhill, D., Marr, L., Kolb, C., Worsnop, D., and Davidovits, P.: Soot particle studies – instrument inter-comparison – project overview, Aerosol Sci. Technol., submitted, 2010.

Hysplit (hybrid single-particle lanrangian integrated trejectory) model access via noaa arl ready (http://wwww.arl.noaa.gov/ready/hysplit4.html). Noaa Air Resources Laboratory, 2003.

Dunlea, E. J., DeCarlo, P. F., Aiken, A. C., Kimmel, J. R., Peltier, R. E., Weber, R. J., Tomlinson, J., Collins, D. R., Shinozuka, Y., McNaughton, C. S., Howell, S. G., Clarke, A. D., Emmons, L. K., Apel, E. C., Pfister, G. G., van Donkelaar, A., Martin, R. V., Millet, D. B., Heald, C. L., and Jimenez, J. L.: Evolution of asian aerosols during transpacific transport in INTEX-B, Atmos. Chem. Phys., 9, 7257–7287, 2009, http://www.atmos-chem-phys.net/9/7257/2009/.

Favez, O., Alfaro, S., Sciare, J., Cachier, H., and Abdelwahab, M. M.: Ambient measurement of light-absorption by agricultural wast burning organic aerosols, Aerosol Science 40, 613–620, 2009.

FIRMS: http://maps.geog.umd.edu/firms/default.asp#, Fire Information for Resource Management Systems, University of Maryland, 2009.

Garland, R. M., Yang, H., Schmid, O., Rose, D., Nowak, A., Achtert, P., Wiedensohler, A., Takegawa, N., Kita, K., Miyazaki, Y., Kondo, Y., Hu, M., Shao, M., Zen, Y. H., Andrae, M. O., and Pöschl, U.: Aerosol optical properties in a rural environment near the mega–city guangzhaou, china: Implications for regional air pollution, radiative forcing and remote sensing, Atmos. Chem. Phys., 8, 5161–5186, 2008, http://www.atmos-chem-phys.net/8/5161/2008/.

Gyawali, M., Arnott, W. P., Lewis, K., and Moosmuller, H.: In situ aerosol optics in reno, nv, USA during and after the summer 2008 California wildfires and the influence of absorbing and non-absorbing organic coatings on spectral light absorption, Atmos. Chem. Phys., 9, 8007–8015, 2009, http://www.atmos-chem-phys.net/9/8007/2009/.

IPCC: The physical science basis. Contribution of working group 1 to the fourth assesment report of the intergovernmental panel on climate change, in, edited by: Solomon, S., Qin, D., Manning, M., Chen, Z., Marquis, M., Averyt, K. B., Tignor, M., and Miller, H. L., Cambridge University Press, Cambridge, United Kingdom and New York, NY, USA, 2007.

Jacobson, M. Z.: Studying the effects of aerosols on vertical photolysis rate coefficient and temperature profiles over an urban airshed, Journal of Geophysical Research, 103(D9), 10593–10,604, 1998.

Lack, D. A. and Cappa, C.: Impact of brown and clear carbon on light absorption enhancement, single scatter albedo and absorption wavelength dependence of black carbon, Atmos. Chem. Phys. Discuss., 10, 785–819, 2010, http://www.atmos-chem-phys-discuss.net/10/785/2010/.

Lewis, K., Arnott, W. P., Moosmöller, H., and Wold, C. E.: Strong spectral variation of biomass smoke light absorption and single scattering albedo observed with a novel dual-wavelength photoacoustic instrument, J. Geophys. Res., 113, D16203,

doi:16210.11029/12007JD009699, 2008.
Myhre, G.: Consistency between satellite-derived and modeled estimates of the direct aerosol effect, Science, 325, 187–190, 2009.
Ramanathan, V. and Carmichael, G.: Global and reginal climate change due to black carbon, Nature Geosciences, 1, 221–227, 2008.
Ruiz-Morales, Y. and Mullins, O. C.: Measured and simulated electronic absorption and emission spectra of asphaltenes, Energy & Fuels, 23, 1169–1177, 2007.
Schauer, J. J., Mader, B. T., Deminter, J. T., Heideman, G., Bae, M. S., Seinfeld, J. H., Flagan, R. C., Cary, R. A., Smith, D., Huebert, B. J., Bertram, T., Howell, S., Kline, J. T., Quinn, P., Bates, T., Turpin, B., Lim, H. J., Yu, J. Z., Yang, H., and Keywood, M. D.: Ace-asia intercomparison of a thermal–optical method for the determination of particle-phase organic and elemental carbon, Environ. Sci. Technol., 37, 993–1001, 2003.
Schwarz, J. P., Spackman, J. P., Fahey, D. W., Gao, R. S., Lohmann, U., Steir, P., Watts, L. A., Thomson, D. A., Lack, D. A., Pfister, L., Mahoney, M. J., Baumgardner, D., Wilson, J. C., and Reeves, J. M.: Coatings and their enhancement of black carbon light absorption in the tropical atmosphere, J. Geophys. Res.-Atmos., 113, D03203, doi:10.1029/2007JD009042, 2008.
Stone, E. A., Lough, G. C., Schauer, J. J., Praveen, P. S., Corrigan, C. E., and Ramanathan, V.: Understanding the origin of black carbon in the atmospheric brown cloud over the indian ocean, Journal of Geophysical Research Atmospheres, 112, D22S23, doi:10.1029/2006JD008118, 2007.
Topping, D., Coe, H., McFiggans, G., Burgess, R., Allan, J., Alfarra, M. R., Bower, K., Choularton, T. W., Decesari, S., and Facchini, M. C.: Aerosol chemical characteristics from sampling conducted on the island of Jeju, Korea during ACE Asia, Atmos. Environ., 38, 2111–2123, 2004.
UN-ECE: http://www.unece.org/env/lrtap, United Nations Economic Comission on Europe, 2009.

Table 1. Aerosol absorption and scattering coefficients, ω_{405}, $Å_{sca}^{405}$, Ångstrom exponents of absorption, with 1 σ standard deviations in parenthesis observed for pollution episodes and background periods during the 2008 CAPMEX field campaign. The background data is taken during the CAPMEX deployment when the Gosan Observatory was not experiencing one of the eight aerosol episodes.

Episode	Dates	β_{abs}^{405}	β_{sca}^{405}	ω_{405}	$Å_{sca}^{405}$	$Å_{abs}$(405/781)	$Å_{abs}$(405/532)
1	3 Aug	10.8 (2.8)	411.2 (187.9)	0.95 (0.09)	1.2 (0.1)	2.2 (0.6)	4.0 (3.6)
2	6–7 Aug	16.6 (5.7)	187.7 (76.8)	0.91 (0.03)	1.5(0.1)	1.8 (0.4)	2.6 (1.8)
3	13–23 Aug	11.0 (6.3)	174.8 (114.5)	0.93 (0.05)	1.5(0.4)	2.1 (1.2)	2.9 (3.5)
4	27–31 Aug	11.5 (5.7)	100.4 (35.8)	0.90 (0.04)	1.7 (0.5)	2.1 (0.8)	3.3 (3.6)
5	3–12 Sep	11.4 (6.0)	103.8 (33.1)	0.90 (0.04)	1.6 (0.4)	2.1 (0.8)	3.6 (3.6)
6	16–20 Sep	12.6 (6.3)	165.7 (100.6)	0.93 (0.05)	1.5 (0.5)	2.0 (1.0)	3.0 (3.3)
7	21–25 Sep	12.5 (6.7)	149.6 (75.9)	0.91 (0.04)	1.3 (0.4)	1.9 (1.0)	2.8 (3.4)
8	27–29 Sep	10.6 (4.6)	41.4 (16.1)	0.79 (0.06)	1.5 (0.9)	2.1 (0.3)	3.8 (3.4)
Bkg.		5.5 (3.6)	34.6 (21.0)	0.84 (0.11)	1.49 (1.3)	2.88 (1.7)	3.13(5.3)

ACPD
10, 9369–9389, 2010

Table 2. Mass data ($\mu g\,m^{-3}$) for Asian pollution transport episodes observed during CAPMEX. The uncertainty represents one standard deviation of the mean reported. The last two columns are composition ratios and are unit-less.

Episode	OC	EC	$PM_{2.5}$	NO_3^-	SO_4^{2-}	OC/SO_4^{2-}	NO_3^-/SO_4^{2-}
1							
2							
3	1.1±0.2	0.1±0.2	48.0±2.8	0.74±0.20	12.3±0.7	0.12±0.02	0.11±0.02
4	1.6±0.2	0.2±0.2	28.5±2.0	1.1±0.20	5.4±0.3	0.31±0.01	0.20±0.01
5	1.7±0.2	0.2±0.2	31.0±2.0	1.2±0.20	5.6±0.3	0.32±0.01	0.23±0.01
6	1.9±0.3	0.3±0.2	33.3±2.2	1.4±0.20	5.0±0.3	0.36±0.02	0.26±0.02
7	1.3±0.2	0.2±0.2	53.8±3.0	1.3±0.20	8.6±0.5	0.15±0.01	0.13±0.01
8	1.5±0.2	0.2±0.2	21.5±1.7	1.9±0.20	2.8±0.2	0.56±0.01	0.69±0.01

ACPD
10, 9369–9389, 2010

Table 3. Mass Absorption Cross Sections (MAC_{total}), brown carbon MAC (MAC_{BrC}), enhancement factor (f), and percent contribution to total absorption [β_{abs}(405 nm) and β_{abs}(532 nm)] for Asian transport episodes observed during CAPMEX.

Episode	MAC_{total}			MAC_{BrC}			f	EC	EC + coat	OC	EC	EC + coat	OC
	405 nm	532 nm	781 nm	405 nm	532 nm	781 nm			405 nm			532 nm	
3	9.0±0.1	4.8±0.1	2.6±0.1	3.4±0.1	1.0±0.1	0.4±0.1	6.0	0.10	0.65	0.34	0.17	0.82	0.17
4	6.0±0.1	3.1±0.1	1.4±0.1	2.6±0.1	0.8±0.1	0.1±0.1	3.5	0.18	0.64	0.36	0.23	0.80	0.19
5	6.3±0.1	2.6±0.1	1.7±0.1	2.5±0.1	0.0±0.1	0.2±0.1	4.3	0.16	0.66	0.34	0.23	0.99	0.01
6	5.0±0.1	2.2±0.1	1.2±0.1	2.1±0.1	0.2±0.1	0.0±0.1	3.0	0.22	0.67	0.32	0.31	0.93	0.07
7	8.5±0.1	4.3±0.1	2.6±0.1	2.8±0.1	0.4±0.1	0.3±0.1	4.3	0.17	0.73	0.27	0.22	0.93	0.13
8	5.6±0.1	1.6±0.2	1.2±0.1	3.4±0.1	0.0±0.2	0.3±0.1	3.2	0.16	0.49	0.51	0.31	0.99	0.01

ACPD
10, 9369–9389, 2010

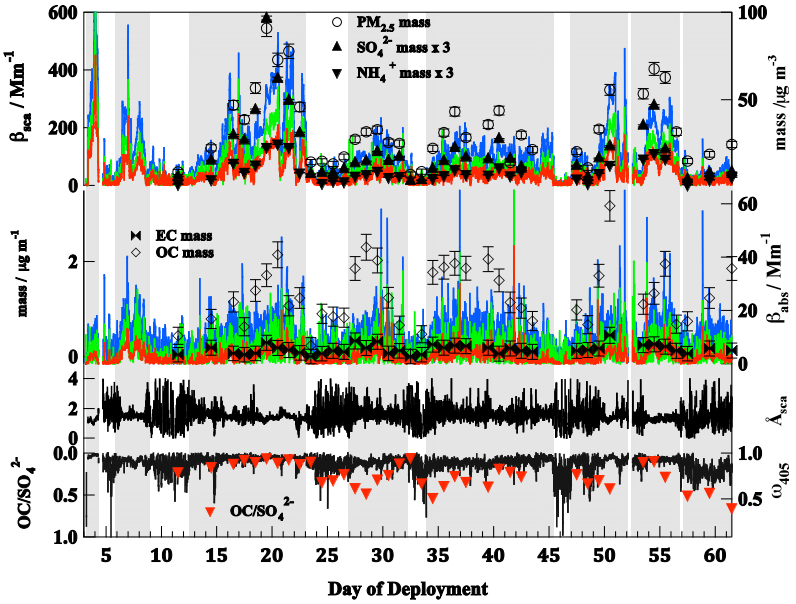

Fig. 1. Temporal profile of aerosol scattering coefficient (β_{sca}), absorption coefficient (β_{abs}), scattering Ångström exponent ($Å_{sca}^{405}$), single scatter albedo at 405 nm (ω_{405}), $PM_{2.5}$ mass, scaled sulfate and ammonium, and elemental and organic carbon masses ($\mu g\,m^{-3}$) for the CAPMEX campaign. The periods highlighted in ash are Asian aerosol transport episodes and their diagnosis as such is discussed in the text. The blue lines represent the 405 nm data, the green line represents the 532 nm data, and the red line represents the 781 nm data.

ACPD
10, 9369–9389, 2010

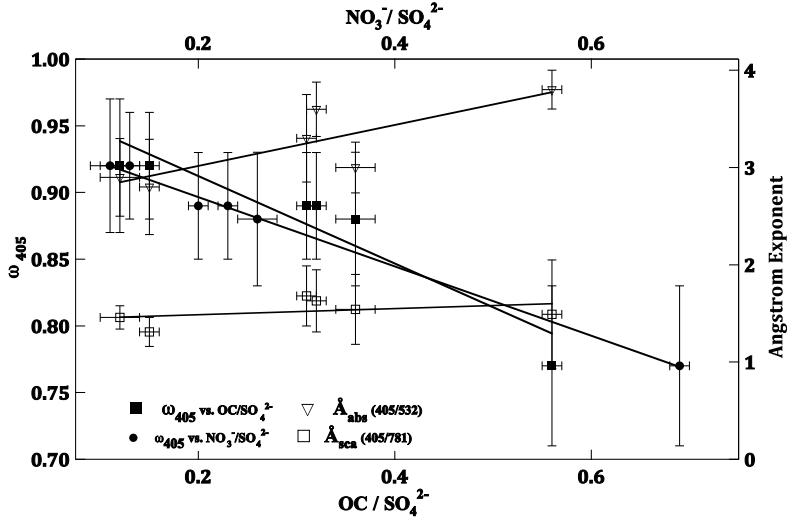

Fig. 2. Single scatter albedo at 405 nm plotted against OC/SO_4^{2-} and against NO_3^-/SO_4^{2-}, $Å_{abs}(405/532)$ plotted vs. OC/SO_4^{2-}, and $Å_{sca}^{405}$ vs. OC/SO_4^{2-} for episodes 3–8 of CAPMEX. The highest ω_{405} occurred for the lowest OC/CO_4^{2-} ratio (0.93 and 0.12; episode 3) and the lowest ω_{405} occurred for the highest OC/SO_4^{2-} ratio (0.79 and 0.56; episode 8).

ACPD
10, 9369–9389, 2010

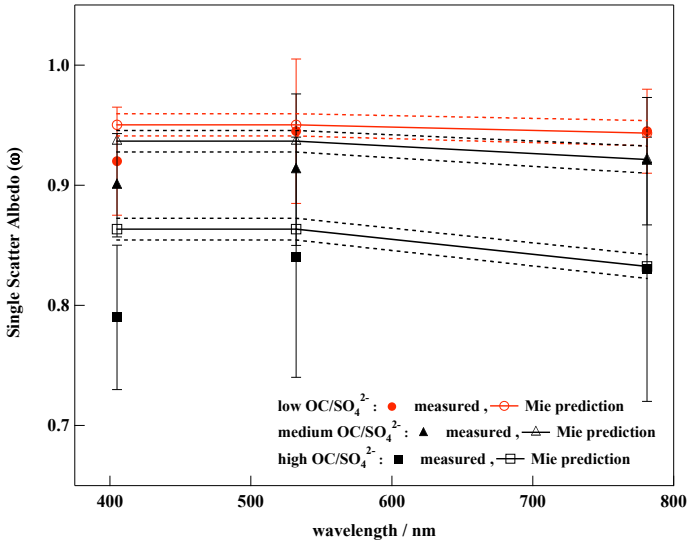

Fig. 3. Single scatter albedo plotted versus wavelength for aerosol episodes classified according to OC/SO_4^{2-} ratios. The classification is discussed in the text. The error bars on the measured ω (solid points) are one standard deviation ω for each episode, representing not the statistical uncertainty of the measurements (which are much smaller), but the real variability within each episode. The predicted ω (open points) represent averaged Mie calculations of ω assuming a wavelength independent index of refraction and forcing the simulation to approach the measured ω_{781} and the measured $\mathring{A}_{sca}^{405}$, the dashed lines represent the ±1 standard deviation for the simulated values (see text for additional detail). Enhanced absorption at short wavelengths with respect to the constant index of refraction model is evident and more significant for the high OC/SO_4^{2-} case.

ACPD
10, 9369–9389, 2010